bioresources.com

Performance of Activated Carbon from *Salvia miltiorrhiza* Roots as the Electrode Material for Supercapacitors

Kui Zhao,[a] Zhengjun Shi,[b] Qiuyuan Li,[c] Qing Li,[a] Fan Gao,[d] and Zhuyun Yan [a,*]

Activated carbons (ACs) were obtained from roots of *Salvia miltiorrhiza* Bunge (Danshen) followed by chemical activation with potassium hydroxide (KOH). The ACs were characterized by nitrogen adsorption, X-ray diffraction (XRD), Fourier transform infrared spectroscopy (FT-IR), scanning electron microscopy (SEM), and electrochemical testing. Results showed that ACs from cultivation sites in Pingyi (ASPY), possessed many micropores, a dominant amount of mesopores, and few macropores. They achieved a value of 1615 m^2/g of specific surface area calculated by the Brunauer-Emmett-Teller (BET) method with numerous oxygen-containing functional groups. Electrodes fabricated with ASPY particles exhibited excellent double-layer specific capacitance (245 F/g), while the other two marked as ASFC (ACs from Fangcheng) and ASZJ (ACs from Zhongjiang) reached values of 163 F/g and 81 F/g, respectively, at a current density of 1 A/g in 6 mol/L KOH electrolytes. Electrodes made by ASPY had a good cyclic stability for 1000 cycles at a potential range from -1 V to 0 V and lower equivalent series resistance (ESR). Meanwhile, the authors found that roots of Danshen that grew in different cultivation sites were remarkably different while they were activated, which was the same with electrochemical properties of the electrodes fabricated by ACs.

*Contact information: a: Pharmacy College, Chengdu University of TCM, 1166 Liutai Road, Chengdu 611137, P. R. China; b: Institute of Chemical Engineering, Southwest Forestry University, Kunming 650224, P. R. China; c: Department of Psychiatry, the First People's Hospital of Honghe State, Mengzi 661199, P. R. China; d: School of Materials Science and Engineering, Yunnan University, Kunming 650091, P. R. China; *Corresponding author: cdtcmyan@126.com*

INTRODUCTION

Energy storage plays a great role in daily life. Important storage devices include batteries and electrochemical capacitors. Supercapacitors, or ECs, are novel devices in the electrical energy storage field, possessing many particular advantages, such as higher specific power density and more durable charge-discharge life than commercial batteries. With a higher specific energy density and working current, the capacitors are extensively used in portable electronics, hybrid power public vehicles of electric energy, pulse power in defense industries or aviation, and uninterruptible power supply (Simon and Gogotsi 2008; Boukhalfa *et al.* 2012).

On the basis of fundamental mechanisms, various carbon materials, such as activated carbons, graphene (Zhang *et al.* 2012), carbon nanotubes (Al-Zubaidi *et al.* 2012), and carbon nanofibers (Kim *et al.* 2011), depend on electrostatic ion adsorption on electrode/electrolyte interface *via* the formation of electric double layers. Hierarchical porous ACs with high Brunauer-Emmett-Teller (BET) areas, especially within a range of 1000 m^2/g to 3000 m^2/g, are the most promising materials to make electrodes for electric

double-layer capacitors (EDLCs) in the supercapacitor industry. This is due to their superior electrochemical stability and electrical conductivity. To develop high-performance supercapacitors, activated carbons (ACs) are extensively activated by physical or chemical methods to improve the specific surface area of the electroactive materials. The AC materials with large specific surface areas are more accessible to electrolyte ions. Therefore, the method concentrates on forming a perfect electric double-layer by optimizing the pore structure, pore size, and chemical bonds in functional groups affiliated on the surface to enrich charge in the electrode/electrolyte interface. The selection of the electrode material is the most important of all links to enhance capacitance of the supercapacitors in mass and volume.
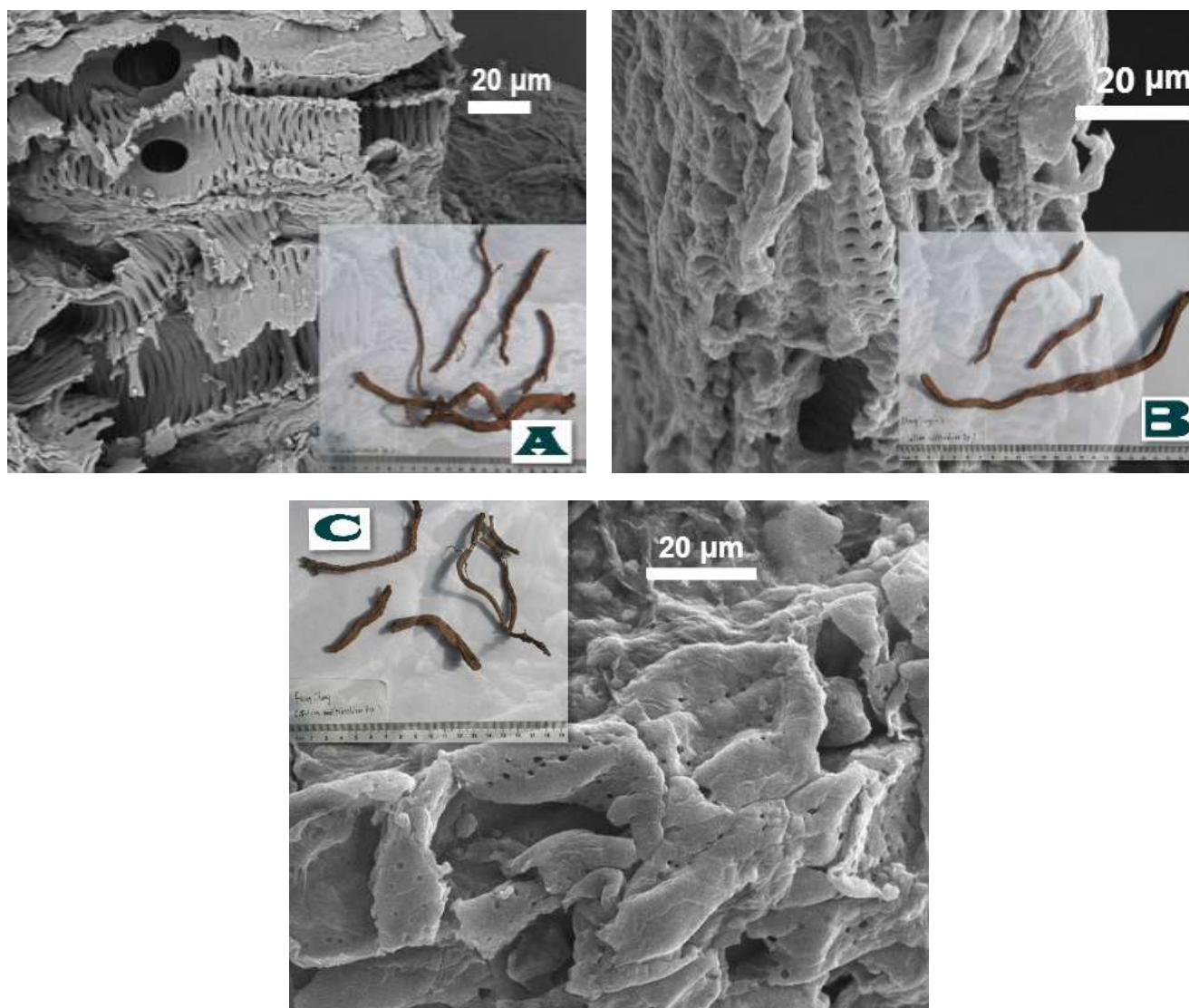
Fig. 1. Digital image of dried SMRs (inset) and the SEM images of extracted raw materials: (a) Pingyi; (b) Zhongjiang; and (c) Fangcheng

To avoid fossil fuel use, researchers increasingly utilize biomass from forestry and crop residues as carbonaceous precursors to obtain ACs, particularly in some agricultural countries with vastly available biomass residues such as fungi (Zhu *et al.* 2011) and banana fibers (Subramanian *et al.* 2007). Those raw botanical materials, including cotton

stalks (Deng *et al.* 2010), corncobs (El-Hendawy 2003), fruit stones, walnut (Aygün *et al.* 2003), and coconut shells (Daud and Ali 2004), are good candidates for low-cost and readily available feedstocks. Each of the previous listed sources, when processed into AC, possesses different surface areas and electrochemical performance.

Compared with the above-mentioned biomass, roots of the medicine plant *Salvia miltiorrhiza* Bunge (Danshen) (SMRs) are abundant in China. Several diploid species belonging to the family Lamiaceae that are native to most regions of China and highly prized are enriched in diterpene compounds due to the presence of the lipid-solubles, known as tanshinones, along with the water-soluble compounds of rosmarinic acid, salvianolic acid, and lithospermic acid (Luo *et al.* 2014). The tanshinones have been shown to promote blood circulation and antiphlogosis, while salvianolic acid has demonstrated efficacy as a treatment for some cardiovascular ailments and acts as a protector against ischemia-reperfusion injury to the brain (Zhou *et al.* 2005). Tanshinones accumulate in the periderm of the reddish roots of *S. miltiorrhiza* specifically (Cui *et al.* 2015). The SMRs contain a great deal of pits and sieve tubes for nutrient transmission, as well as a large number of vessels and cellulose in the tissue, as shown in Fig. 1. Simultaneously, in Fig. 1(a) were longer diameters in width and thinner walls of vessels with more closely reticulated structure than others. There were lots of amorphous cellulose revolving around vessels in Fig. 1(b). As shown in Fig. 1(c) rows of small round holes are distinctly distributed on the wall of vessels.

The authors believe that the specific structure leads to the generation of the pores after carbonization, and these pores are conducive to prepare the porous AC through KOH activation at high temperatures (Ahmadpour and Do 1996; Deng *et al.* 2010). Herein, ACs were synthesized from the SMRs by carbonization and chemical activation with potassium hydroxide. The morphology, pore structure, and specific surface area of the ACs were detected by scanning electron microscopy (SEM) and BET methods. Furthermore, crystalline structure and oxygen functionality on the surface of carbon were measured using X-ray diffraction (XRD) and Fourier transform infrared (FT-IR) spectroscopy. Finally, the performance on electrochemistry was detected *via* cyclic voltammetry (CV), galvanostatic charge/discharge (GCD), and electrochemical impedance spectroscopy (EIS) in KOH electrolyte.

EXPERIMENTAL

Materials

Synthesis of activated carbon

The SMR was collected from three different cultivation sites (Pingyi, Fangcheng, and Zhongjiang, China). Each sample was sieved to small pieces between 0.5 cm to 1 cm, and extracted by 95% ethanol for 2 h, then hot water for 2 h, and washed by distilled water three times to obtain herb residues. The three residues of SMRs were dried at 105 °C for 6 h, and then soaked in KOH with a blending ratio of 3:1 wt% for 2 h. The mixture was dried at 105 °C, and then placed in a furnace heated to 850 °C at the rate of 5 °C/min with a constant N_2 (99.99%) flow of 300 cm^3/min. The activating process was maintained for 2 h. The product was immersed with 1 mol/L HCl along with ultra-pure water repeatedly until a neutral pH was achieved. Finally, the active substance marked as either ASPY (precursors from Pingyi), ASFC (precursors from Fangcheng), or ASZJ (precursors from

Zhongjiang), was ground, sieved to a particle size of 220-mesh, and then placed at 105 °C for approximately 2 h for further analysis. The yield of the active product was defined as the weight in the last round. The percent value was calculated from Eq. 1,

$$Y(\%) = \frac{m}{M} \times 100$$

(1)

where *m* and *M* are the dry weight (g) of the activated carbon and the precursor, respectively.

Electrode fabricated

The negative electrodes were prepared by following the method reported by Lang *et al.* (2012). Typically, 80% mass fraction of activated carbon material was blended with 7.5% of acetylene black (> 99.9%) along with 7.5% of conducting graphite in a mortar until homogeneous black powder was obtained. Then, 10% of 60% polytetrafluoroethylene was quickly added into this mixture with a few drips of ethanol as the disperser. After the evaporation came to an end at room temperature, the precast sheet was pressed at 10 MPa and wrapped in sulfate paper into a nickel foam (pretreated with 6 M HCl) of 1 cm × 2 cm. Thus, each electrode had an active area of approximately 1 cm^2 that made the calculation shortcut. The pressed electrodes were weighed after being oven-dried for 24 h at 80 °C.

Methods

Characterization of structure

The features of the activated products, particularly morphology and microstructure, were detected under a field emission scanning electron microscope (FESEM; Novanano 450; FEI, Hillsboro, OR, USA). Crystallite structures were analyzed by a powder X-ray diffractometer (XRD; Empyrean, PANalytical, Almelo, Netherlands) with Cu K_α radiation from 5 ° to 90 °. The chemical characteristics of the SMR-based carbon materials were analyzed with an FT-IR spectrometer (Nicolet IS10; Thermo Fisher, Waltham, USA). The samples were performed on a nitrogen adsorption-desorption isotherm measurement (ASAP 2020 Plus analyzer, Micrometitics, Atlanta, GA, USA) at 77 K. All samples underwent a degassing process at 300 °C for 6 h to take the surface gaseous contaminants off before the adsorption/desorption experiments. The BET method was used to compute the specific surface area individually, and the pore volume as a whole was estimated from the value adsorbed at the relative pressure of $P/P_0 = 0.99$. The pore width distributions of the three ACs were calculated *via* density functional theory (DFT) measurement (Li *et al.* 2011).

Boehm's acidity

To evaluate the acidic and basic properties of each of the surface modified activated carbons, a scheme suggested by Boehm that measures the amount of acid/base uptake by carbon by neutralizing titration was followed (Noh and Schwarz 1990). The reagents used were HCl, NaOH, NaHCO$_3$, and Na$_2$CO$_3$ solutions. Four parts, about 100 mg each in weight, of a sample were placed in four separate glass bottles containing 20 mL of 0.05 mol/L solution of each reagent mentioned. The containers were gently shaken for 24 h on a Shoker (TS-100B, Bozhen Corporation, Shanghai, China). The solutions were then filtered with filter paper. The amount of each reagent adsorbed was determined by back

titration of the solution. Hydrochloric acid was the titer for the three basic solutions, and sodium hydroxide was used to titrate the hydrochloric acid solution.

Point of zero charge (PZC)

To measure the PZC of the samples, three different initial pH solutions were prepared using 0.1 mol/L HNO_3 and 0.1 mol/L NaOH; for example, pH = 3, 6, or 11. Six bottles were filled with 20 mL of the solution, and different amounts of carbon sample were added (0.05 g, 0.25 g, 0.5 g, 1.0 g, 2.0 g, 2.5 g) each initial pH (Noh and Schwarz 1990). The equilibrium pH was measured after being shaken for 24 h on a pH-meter (CT-6021A, Liyuan Corporation, Shenzhen, China).

Electrochemical tests in a three-electrode system

Electrodes were immersed in 6 mol/L KOH electrolytes for 12 h to make electrolyte ions sufficiently diffuse into the porous carbon.

All of the tests of each electrode were performed on an electrochemical working station (CHI660D; Chenhua Instrument Co., Ltd., Shanghai, China) at room temperature. A platinum slice electrode (9 cm^2) served as the positive, a saturated calomel electrode served as the reference electrode, and the working electrode served as the negative, correspondingly.

The GCD was underway at current densities from 0.5 A/g to 10 A/g. The CV measurements were conducted at a sweeping rate that ranged from 5 mV/s to 100 mV/s. Electrochemical impedance spectroscopy (EIS) tests collected data from 100 kHz to 10 mHz with an alternate current amplitude of 5 mV. The specific capacitance was calculated from Eq. 2,

$$C(F/g) = \frac{I}{\frac{\Delta V}{\Delta t}m} = \frac{I\Delta t}{\Delta V m}$$

(2)

where C is the specific capacitance (F/g), I is the value of the constant current, ΔV and Δt stand for the window of the potential and times of discharging in one cycle (s), and m is the mass (g) of the corresponding electrode material. The coulombic efficiency was calculated from Eq. 3,

$$\eta(\%) = \frac{t_d}{t_c} \times 100$$

(3)

where t_d and t_c are discharging and charging time (s) of one cycle, respectively.

RESULTS AND DISCUSSION

Microstructure Characterizations of AC Materials

Porous carbon materials were synthetized by KOH activating the carbonaceous precursor.

When the temperature was increased to over 700 °C, the plausible products of the activation reactions could include the carbon dioxide, hydrogen, carbon monoxide, potassium oxide, potassium carbonate, and metallic potassium carbonization and oxidation conditions (El-Hendawy 2006).

The following reactions take place between KOH and carbon (Marsh and Rodríguez-Reinoso 2006):

First: $6KOH + 2C = 2K + 3H_2 + 2K_2CO_3$ (4)

Second: $K_2CO_3 + 2C = 2K + 3CO$ (5)

Third: $K_2CO_3 = K_2O + CO_2$ (6)

The results of the percent yield of SMRs carbon are listed in Table 1. The yield of ASPY was 15.1% less than that of ASZJ. Images of SMRs carbon are displayed in Fig. 2. They showed some bumps and rough microstructure for the three ACs material in this paper.

After chemical activation, the AC samples exhibited a texture composed of particles on the surface of carbon materials with differences between individuals. Although the activated primary structure with pores of all three ACs in the mixed electrode materials was broken, the mixture of ASPY and ASFC with porous and open cell active particles diffused while the samples of ASZJ particles (shown in Fig. 2(b)) were visibly dense and smooth.
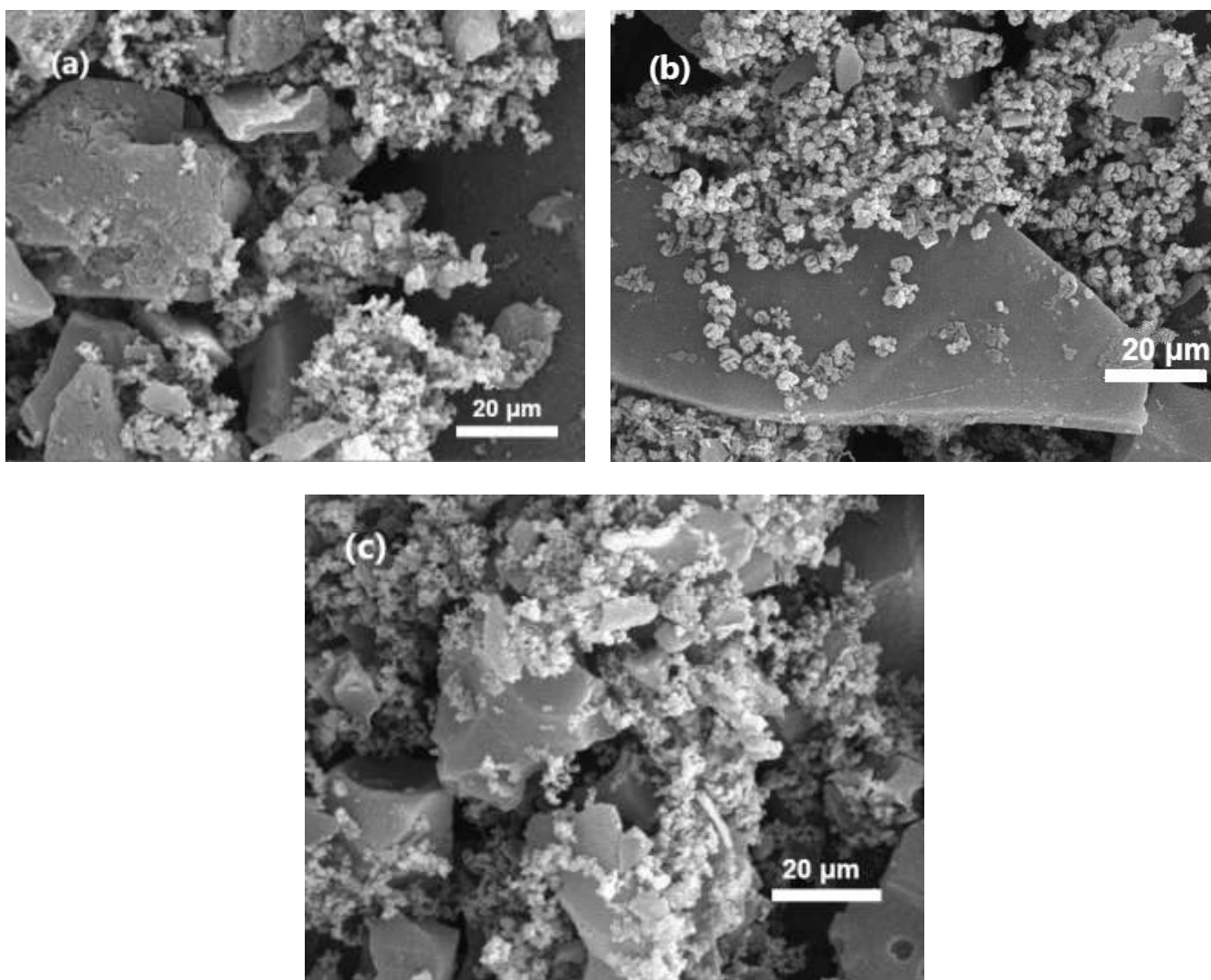
Fig. 2. SEM of electrode materials: (a) ASPY; (b) ASZJ; and (c) ASFC

bioresources.com

Nitrogen adsorption-desorption isotherms of both SMR-based carbon materials at 77 K are shown in Fig. 3(a). All samples were represented with the characteristic of type IV. The sharp increase at low relative pressure was attributed to the existence of micropores, and the desorption hysteresis at medium relative pressure suggests the presence of developed mesoporosity (Bansal and Meenakshi 2005). Furthermore, the results were observed from the pore size distribution in Fig. 3(b). The porous material of ASPY consisted mostly of micropores and mesopores. The mesoporous rate was calculated as 71%, 68%, and 44% in ASPY, ASFC, and ASZJ, respectively. However, in contrast, Fig. 3(b) illustrates that AC material was composed of mesopores and macropores. As shown in Fig. 4 and Table 1, the shapes for ASZJ, ASPY, and ASFC were very distinctive, and the specific surface area of ASPY (1615 m^2/g) was higher than that of ASFC (1487 m^2/g) and ASZJ (525 m^2/g). Meanwhile, an apparent increase in pore volume was observed from 0.341 cm^3/g for ASZJ to 0.997 cm^3/g for ASPY in Table 1, which indicated that the activation reactions proceeded faster at ideal precursors and more pore channels were developed. Additionally, those pore widths between approximately 0.8 nm and 1 nm occupied almost all of the micropores in ASZJ from data of pore width distribution.

Table 1. Textural Characteristics and Yield of ACs

Sample	S_{BET} (m^2/g)	S_{Mes} (cm^2/g)	V_{Mic} (cm^3/g)	V_{Mes} (cm^3/g)	D_{Ap} (nm)	Yield (%)
ASPY	1615	1160	0.2884	0.7084	2.589	20.82
ASFC	1487	935	0.2766	0.5790	2.301	26.71
ASZJ	525	169	0.1853	0.1557	2.593	35.90

Values are the average of three replications; S_{BET}- total area; S_{Mes}- area of mesopores; V_{Mic} and V_{Mes}- micro- and mesopore volumes; and D_{Ap}- average pore radius
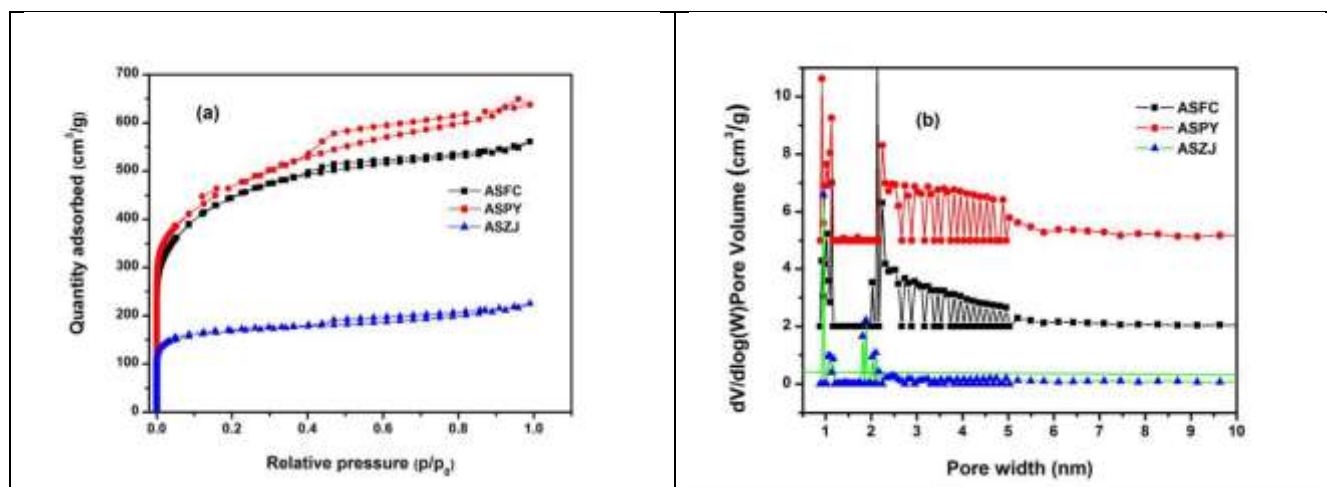
Fig. 3. (a) Nitrogen adsorption-desorption isotherms of the ASFC, ASPY, and ASZJ samples; (b) Pore size distributions of the ASFC, ASPY, and ASZJ samples

Characteristics of ACs and Function Groups

The FT-IR spectra are shown in Fig. 4(a) for the carbonized ASPY, ASFC, and ASZJ samples activated with KOH of the three carbon materials. The carbon materials of ASPY and ASFC possessed similar chemical structural characteristics, which indicated more intense infrared peaks compared to the ASZJ sample with KOH activation. Based on

bioresources.com

Boehm's acidity and PZC analysis in Table 2, the order of oxygen groups content was phenolic > carboxyl > lactonic group. Meanwhile, the order of acid oxygen groups contents in total was ASFC > ASPY > ASZJ. Combined with pH_{PZC} value, ACs could defined as acido-basic property because of certain number of acid oxygen groups. In FT-IR spectra, the O-H stretching vibration (3436 cm^{-1}) and the bending vibration (1630 cm^{-1}) were due to surface hydroxyl groups and bound water, indicating that the O-H groups rounded into hydrogen bonds as reported (El-Hendawy 2006). Thus the ASPY and ASFC samples might have a higher probability to attract alkaline electrolyte than the ASZJ samples. Noticeable changes contrasted by ASZJ were also found in the spectra of the ASPY and ASFC samples. Although, all the strong peaks at 3500 cm^{-1} might be partly due to samples that were not dry enough.

Table 2. Contents of Acid Oxygen Groups on the Carbon Surface and pH_{PZC}

Sample	Carboxyl (mmol/g)	Lactonic (mmol/g)	Phenolic (mmol/g)	Total (mmol/g)	PH_{PZC}
ASPY	0.463	0.138	0.774	1.375	3.75
ASFC	0.562	0.213	0.750	1.525	3.45
ASZJ	— —	0.250	0.225	0.575	6.74
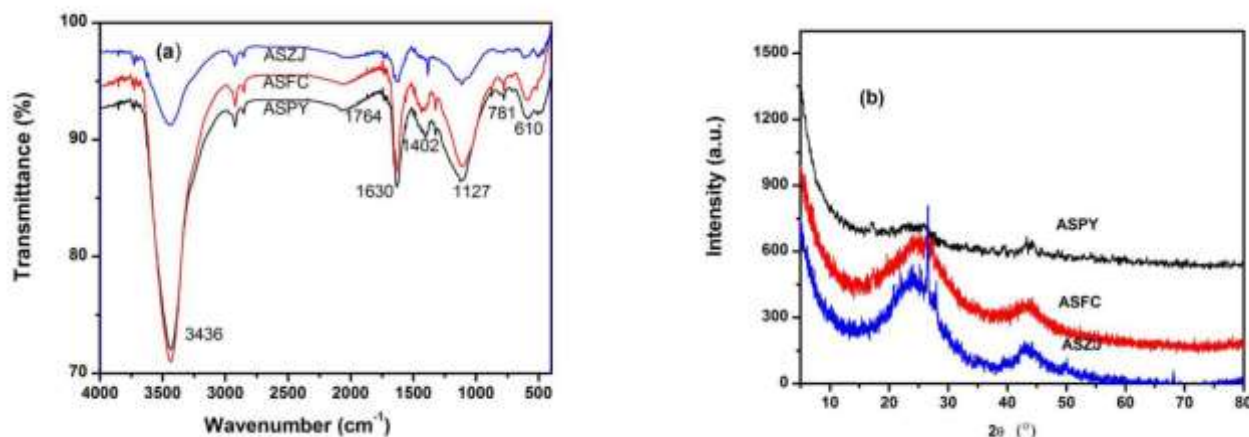
Fig. 4. Pingyi (ASPY), Fangcheng (ASFC), and Zhongjiang (ASZJ) carbon samples: (a) FT-IR spectra; (b) XRD patterns

The region of 2950 cm^{-1} to 2800 cm^{-1} was the stretching vibration of the aromatic and aliphatic C-H, as was shown on the assembling of active functional groups on the carbon surfaces of all carbon samples. Compared with the vibration of an aromatic C=C bond at 1402 cm^{-1} present in ASPY and ASFC samples, the infrared vibration of C=C bond for the AC sample shifted to a lower wavenumber due to the reaction of KOH and carbon materials. These results demonstrated that both carbons possessed a great deal of oxygen functional groups on the surface of the materials. It is known that the aggregation (C-O and O-C=O) is active in the alkaline electrolyte (Khomenko *et al.* 2010). The band located at 1127 cm^{-1} was attributed to the infrared vibration of the C-O bending vibrations in the form of these pryone-like rings (Smets *et al.* 2016). Many of these C-C and C-O revolved around to form stable rings similar to those that exist in a phenolic resin (Trick and Saliba 1995). Meanwhile, the promoted polyaromatic structures where sharp bands occurred were due to

C-H groups that were represented. Thus, 781 cm^{-1} and 610 cm^{-1} indicated the deformation vibration of the aromatic C-H in ASPY and ASFC, but in ASZJ the peak was less intense in the region and almost disappeared.

Surprisingly, no strong band between 1720 cm^{-1} and 1700 cm^{-1} denoting the presence of carboxylic acid groups (COOH) in the samples was detected in the infrared spectra. This fact was worth mentioning, as such oxygenic surface groups were frequently found in AC, showing activity in the adsorption of metal ions from the liquid phase (Mendoza-Carrasco *et al.* 2016).

Features of powder XRD measurements of the three samples are shown in Fig. 4(b). In the profiles, AC samples possessed two broad diffraction peaks at approximately 2θ (approximately 24.7 ° and 43.8 °), which were attributed to the (002) and (100) crystal planes. After KOH activation for the SMRs material, the peak of (002) planes had obviously broadened, the ASPY sample had almost disappeared, and the (100) reflection plane was still present in the sample. The ASPY material had a considerable intensity in the low-angle scatter, which suggested the existence of a great deal of amorphous substance. Compared with ASPY, there was a salient region in the intensity of the peaks for the ASFC (002) with part of the graphitized amorphous structure. The ASZJ (002) behaved similarly. Moreover, nearby 26° sharp peaks of crystal appeared. These demonstrated non-ideal porosity or inorganic impurity that would be preserved.

Electrochemical Tests for Carbon Electrodes in Three-electrode System

The typical three-electrode method was chosen to determine the electrochemical performance of the carbon materials that were spread on nickel foam in KOH electrolyte. As shown in Fig. 5, the CV and GCD curves were used to characterize the capacitive behavior of precast ASFC, ASPY, and ASZJ electrodes in 6 mol/L KOH electrolyte.

The CV curves of the negative electrodes in the experiment were shown as relatively rectangular in Fig. 5(a), which indicated that most of the ion charges were stored by the electric double-layer mechanism for electrodes (Fang *et al.* 2013). At the same time, the area of ASPY electrode was the highest among itself, ASFC, and ASZJ, which suggested that the ASPY electrode possessed the highest specific capacitance. Moreover, the results of the GCD process for the three carbon materials at current density of 1 A/g are shown in Fig. 5(b). The specific capacitances were 245 F/g, 163 F/g, and 81 F/g, which corresponded to the storage capacity of the three ACs. The specific capacitances of ASPY and ASFC were higher than that of ASZJ in KOH electrolyte at the same current density of 1 A/g, which might have been attributed to the ideal hierarchical porous structure in ASPY, including the domination of the micropores and mesopores (Chmiola *et al.* 2006). However, the few mesopores present led to the low specific capacitance for the ASZJ electrode.

The porous structures of ASPY were conducive to generating the compact electric double layer and excellent transmission channel of the electrolyte ions on the surface of carbon materials. The CV curves are shown in Fig. 6a. The GCD curves at the current density range from 0.5 A/g to 10 A/g exhibited good triangle shapes, excellent capacitance retention, and the specific capacitance of 255 F/g and 237 F/g at the current density of 0.5 and 2.5 A/g, respectively, in Fig. 6(b). The capacitance retention was as high as 93%, which indicated the rapid charge and discharge capability for the ASPY electrodes. The capacitance of a single electrode in symmetric EDLC was approximately four times that of the two-electrode symmetric cell if a supercapacitor was fabricated with the working electrodes (Cao *et al.* 2017).
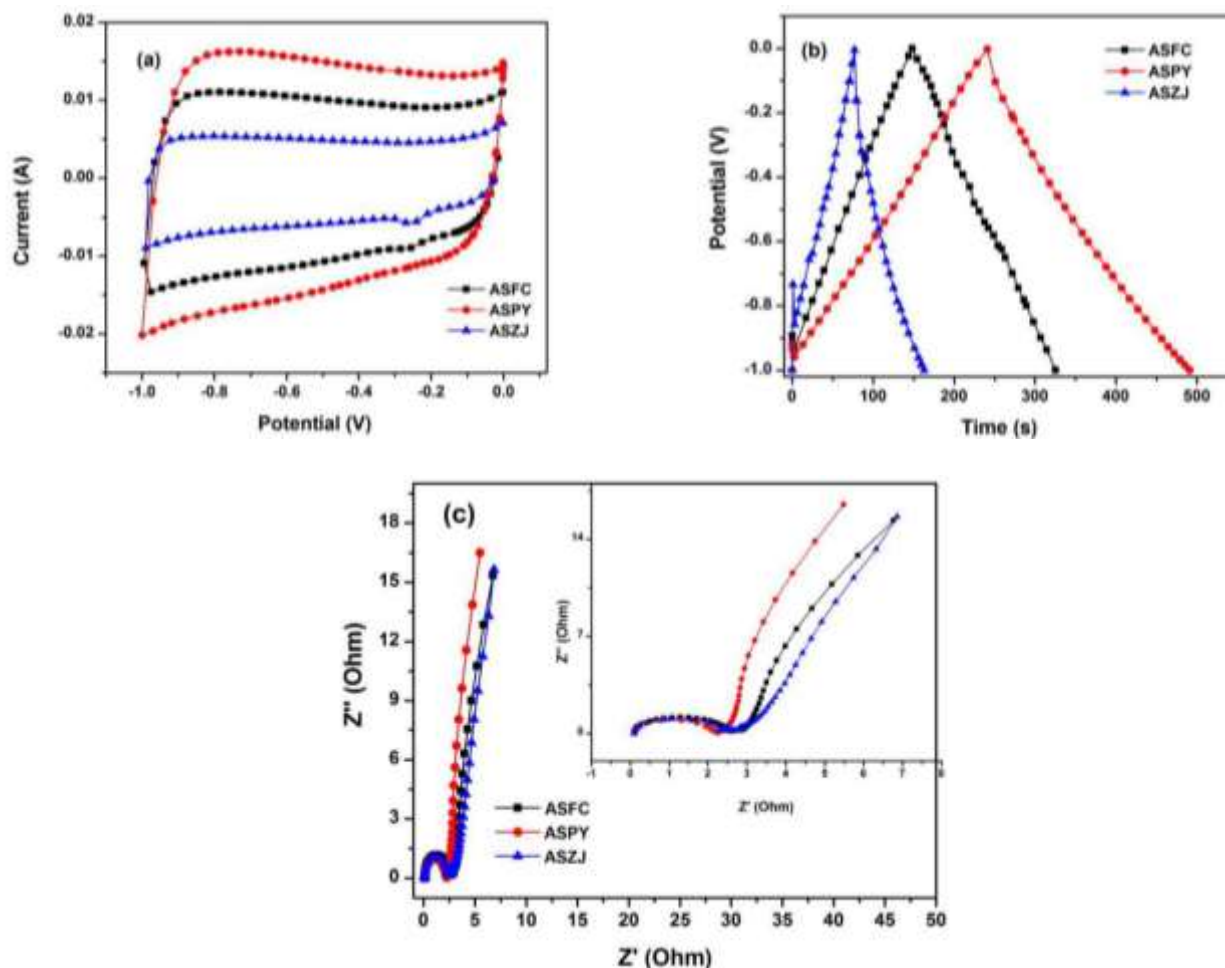
Fig. 5. Electrochemical tests for carbon electrodes of ASPY, ASFC, and ASZJ: (a) at a sweep rate of 10 mv/s; (b) a current density of 1 A/g; and (c) Nyquist plot and high-frequency region inset

Electrochemical impedance spectroscopy was used to investigate the performances of the supercapacitor in the frequency range of l00 kHz to 10 mHz, such as frequency response and equivalent series resistance (ERS) (Inal *et al.* 2015).

The value of ERS was 0.71 Ω from the Nyquist plot in Fig. 6(c) for ASPY-based electrodes.

The low ERS and small Warburg diffusion resistance of 1.20 Ω resulted from the hierarchical porous structure and numerous oxygen function groups of ASPY, which was prepared *via* carbonization and the KOH activation process of SMRs.

As shown in Fig. 6(c), ASPY electrodes presented ideal impedance characteristics because the semicircle of small radius was obtained at a high-frequency range (inset) due to low electronic resistance between the activated carbon material, and the near vertical Warburg diffusion segment at low-frequency range attributed to the ions diffusion in the structure of the electrodes.
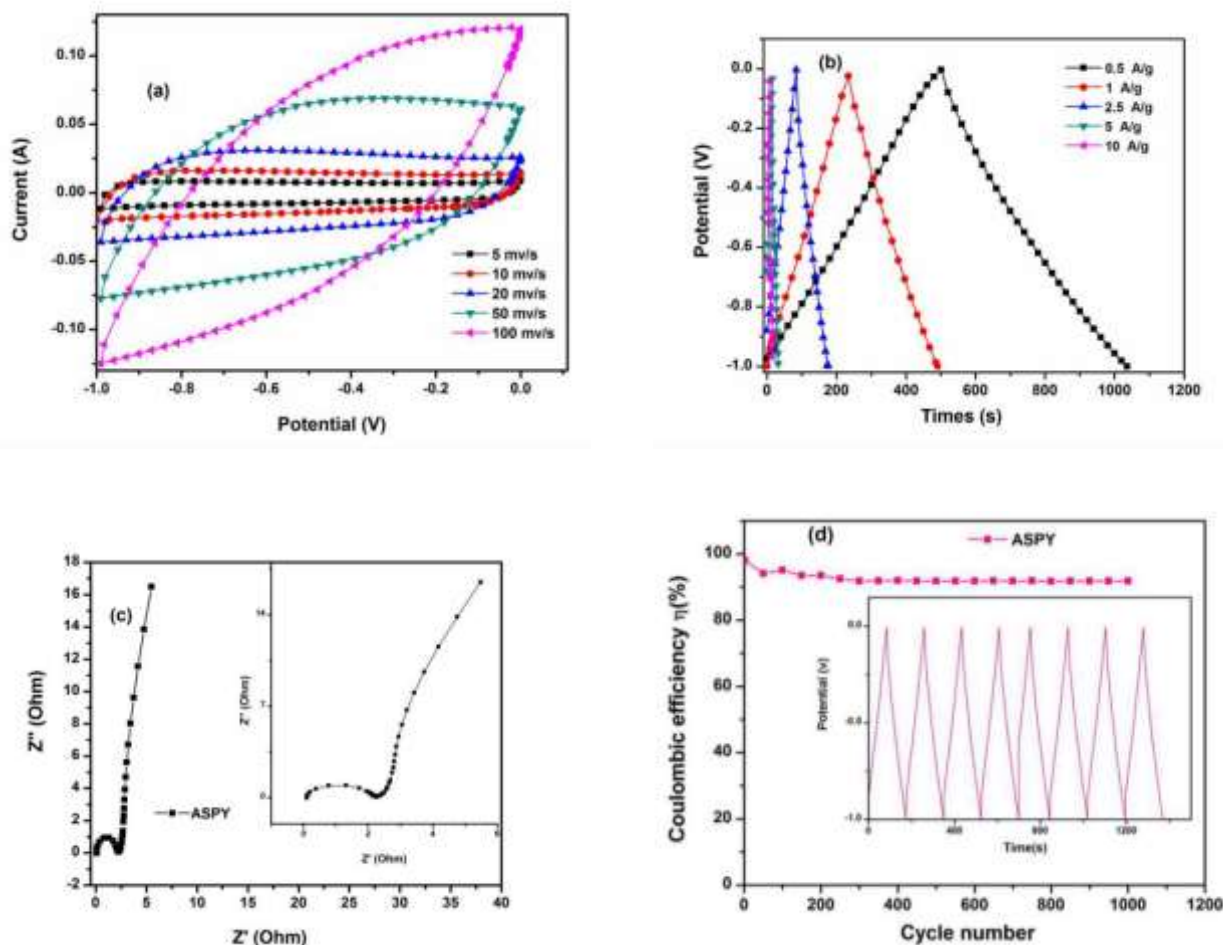
Fig. 6. Electrochemical tests for carbon electrodes of ASPY: (a) at a range rate of 5 mv/s,10 mv/s, 20 mv/s, 50 mv/s, and 100 mv/s; (b) a current density of 0.5 A/g,1 A/g, 2.5 A/g, 5 A/g, and 10 A/g; (c) Nyquist plot from 100 k to 10 mHz, where inset is high-frequency region; (d) relationship between capacitance retention and cycle number of ASPY at current density of 2.5 A/g, where inset is the final eighty cycles

The specific capacitance of ASPY electrodes obtained using GCD analysis data at various current densities remained relatively stable at a value less than 2.5 A/g. The ASPY electrodes underwent a charge-discharge cycle in the potential range from -1.0 V to 0 V at a constant current density of 2.5 A/g to obtain stability data.

There was a slight loss of capacitance in the first 100 cycles due to the irreversible reaction between the electrolyte and electrodes, and then remained almost constant quantized by coulombic efficiency (η) in Fig. 6(d).

The primary capacitance decreased 7.2% for ASPY electrodes after 2000 charge-discharge processes. For the final eight cycles, the charge-discharge curve exhibited perfect linearity, and the charging and discharging time had similar equality, shown in the Fig. 6(d) inset.

Thus, the material for electrodes activated by KOH possessed good stability with various current densities and durability of cycles.

bioresources.com

CONCLUSIONS

1. The activated carbons (ACs) from dried roots of *Salvia miltiorrhiza* Bunge (Danshen) (SMR) were successfully prepared by pyrolysis followed by KOH activation at a low ratio (3:1). Hierarchical porous carbons exhibited a grainy texture, numerous oxygen-containing functional groups on the surface with a specific surface area up to 1615 m^2/g, and could be further improved.

2. Electrochemical results suggested that ACs from cultivation sites in Pingyi (ASPY) had the best capacitive behavior with rectangular and triangular characteristics that corresponded to the CV, GCD, and EIS curves. The ASPY possessed high surface area, an ideal mesoporous rate of 71%, numerous hydrogen bonds, and oxygen-containing function groups.

3. The SMR is a new precursor for high-quality ACs for electrochemical capacitors due to its high-specific capacitance, low ESR and Warburg diffusion resistance, and good stability with various current densities and durability of cycles.

4. Meanwhile, it was also found that roots of *S. miltiorrhiza* Bunge (Danshen) from different cultivation sites were considerably different once they were activated, and the same occurred with the electrochemical properties of the electrodes fabricated by ACs.

The results showed that our research had found the optimization precursors of activated carbon for supercapacitors. The medical value of SMRs bring great economic benefits, which have encouraged farmers to plant these medical herbs. The yield after the extraction process from the pharmaceutical factory was composed of an abundant source of raw materials but the therapeutic effect benefits from the chemical composition vary greatly among the roots from different cultivation sites, as was reported. The different growing environment correlated with the microcosmic biological structures and carbon performance. Furthermore, the way in which the environment led to these differences remain to be studied.

ACKNOWLEDGMENTS

REFERENCES CITED

Ahmadpour, A., and Do, D. (1996). "The preparation of active carbons from coal by chemical and physical activation," *Carbon* 34(4), 471-479. DOI: 10.1016/0008-6223(95)00204-9

Al-Zubaidi, A., Inoue, T., Matsushita, T., Ishii, Y., Hashimoto, T., and Kawasaki, S. (2012). "Cyclic voltammogram profile of single-walled carbon nanotube electric double-layer capacitor electrode reveals dumbbell shape," *J. Phys. Chem. C* 116(14), 7681-7686. DOI: 10.1021/jp300802z

Aygün, A., Yenisoy-Karakaş, S., and Duman, I. (2003). "Production of granular activated carbon from fruit stones and nutshells and evaluation of their physical, chemical and

adsorption properties," *Micropor. Mesopor. Mat.* 66(2-3), 189-195. DOI: 10.1016/j.micromeso.2003.08.028

Bansal, R. C., and Meenakshi, G. (2005). *Activated Carbon Adsorption*, Taylor and Francis/CRC, Boca Raton, FL, USA.

Boukhalfa, S., Evanoff, K., and Yushin, G. (2012). "Atomic layer deposition of vanadium oxide on carbon nanotubes for high-power supercapacitor electrodes," *Energy & Environmental Science* 2012(5), 6872-6879. DOI: 10.1039/c2ee21110f

Cao, L., Tang, G., Mei, J., and Liu, H. (2017). "Construct hierarchical electrode with $Ni_xCo_{3-x}S_4$ nanosheet coated on $NiCo_2O_4$ nanowire arrays grown on carbon fiber paper for high-performance asymmetric supercapacitors," *J. Power Sources* 359, 262-269. DOI: 10.1016/j.jpowsour.2017.05.051

Chmiola, J., Yushin, G., Dash, R., and Gogotsi, Y. (2006). "Effect of pore size and surface area of carbide-derived carbons on specific capacitance," *J. Power Sources* 158(1), 765-772. DOI: 10.1016/j.jpowsour.2005.09.008

Cui, G., Duan, L., Jin, B., Qian, J., Xue, Z., Shen, G., Snyder, J., Song, J., Chen, S., Huang, L., *et al.* (2015). "Functional divergence of diterpene syntheses in the medicinal plant *Salvia miltiorrhiza*," *Plant Physiol.* 169(3), 1607-1618. DOI: 10.1104/pp.15.00695

Daud, W., and Ali, W. (2004). "Comparison on pore development of activated carbon produced from palm shell and coconut shell," *Bioresource Technol.* 93(1), 63-69. DOI: 10.1016/j.biortech.2003.09.015

Deng, H., Li, G., Yang, H., Tang, J., and Tang, J. (2010). "Preparation of activated carbons from cotton stalk by microwave assisted KOH and K_2CO_3 activation," *Chem. Eng. J.* 163(3), 373-381. DOI: 10.1016/j.cej.2010.08.019

El-Hendawy, A.-N. (2003). "Influence of HNO_3 oxidation on the structure and adsorptive properties of corncob-based activated carbon," *Carbon* 41(4), 713-722. DOI: 10.1016/S0008-6223(03)00029-0

El-Hendawy, A.-N. (2006). "Variation in the FTIR spectra of a biomass under impregnation, carbonization and oxidation conditions," *J. Anal. Appl. Pyrol.* 75(2), 159-166. DOI: 10.1016/j.jaap.2005.05.004

Fang, B., Bonakdarpour, A., Kim, M.-S., Kim, J., Wilkinson, D., and Yu, J.-S. (2013). "Multimodal porous carbon as a highly efficient electrode material in an electric double layer capacitor," *Micropor. Mesopor. Mat.* 182, 1-7. DOI: 10.1016/j.micromeso.2013.08.007

Inal, I., Holmes, S., Banford, A., and Aktas, Z. (2015). "The performance of supercapacitor electrodes developed from chemically activated carbon produced from waste tea," *Appl. Surf. Sci.* 357, 696-703. DOI: 10.1016/j.apsusc.2015.09.067

Khomenko, V., Raymundo-Piñero, E., and Béguin, F. (2010). "A new type of high energy asymmetric capacitor with nanoporous carbon electrodes in the aqueous electrolyte," *J. Power Sources* 195(13), 4234-4241. DOI: 10.1016/j.jpowsour.2010.01.006

Kim, B.-H., Yang, K., Kim, Y. A., Kim, Y. J., An, B., and Oshida, K. (2011). "Solvent-induced porosity control of carbon nanofiber webs for supercapacitor," *J. Power Sources* 196(3), 10496-10501. DOI: 10.1016/j.jpowsour.2011.08.088

Lang, J.-W., Yan, X.-B., Liu, W.-W., Wang, R.-T., and Xue, Q.-J. (2012). "Influence of nitric acid modification of ordered mesoporous carbon materials on their capacitive performances in different aqueous electrolytes," *J. Power Sources* 204, 220-229. DOI: 10.1016/j.jpowsour.2011.12.044

Li, X., Xing, W., Zhuo, S., Zhou, J., Li, F., Qiao, S.-Z., and Lu, G.-Q. (2011). "Preparation of capacitor's electrode from sunflower seed shell," *Bioresource. Technol.* 102(2), 1118-1123. DOI: 10.1016/j.biortech.2010.08.110

Luo, H., Zhu, Y., Song, J., Xu, L., Sun, C., Zhang, X., Xu, Y., He, L., Sun, W., Xu, H., *et al.* (2014). "Transcriptional data mining of *Salvia miltiorrhiza* in response to methyl jasmonate to examine the mechanism of bioactive compound biosynthesis and regulation," *Physiol. Plantarum* 152(2), 241-255. DOI: 10.1111/ppl.12193

Marsh, H., and Rodríguez-Reinoso, F. (2006). "Activation processes (chemical)," in: *Activated Carbon*, Elsevier Science Ltd., Amsterdam, Netherlands. DOI: 10.1016/B978-008044463-5/50020-0

Mendoza-Carrasco, R., Cuerda-Correa, E., Alexandre-Franco, M., Fernández-González, C., and Gómez-Serrano, V. (2016). "Preparation of high-quality activated carbon from polyethyleneterephthalate (PET) bottle waste. Its use in the removal of pollutants in aqueous solution," *J. Environ. Manage.* 181, 522-535. DOI: 10.1016/j.jenvman.2016.06.070

Noh, J., and Schwarz, J. (1990) "Effect of HNO_3 treatment on the surface acidity of activated carbons," *Carbon* 28(5), 675-682. DOI: 10.1016/0008-6223(90)90069-B

Simon, P., and Gogotsi, Y. (2008) "Materials for electrochemical capacitors," *Nat. Mater.* 7, 845-854. DOI: 10.1038/nmat2297

Smets, K., de Jong, M., Lupul, I., Gryglewicz, G., Schreurs, S., Carleer, R., and Yperman, J. (2016). "Rapeseed and raspberry seed cakes as inexpensive raw materials in the production of activated carbon by physical activation: Effect of activation conditions on textural and phenol adsorption characteristics," *Materials* 9(7), 565-573. DOI: 10.3390/ma9070565

Subramanian, V., Luo, C., Stephan, A., Nahm, K., Thomas, S., and Wei, B. (2007). "Supercapacitors from activated carbon derived from banana fibers," *J. Phys. Chem. C* 111(20), 7527-7531. DOI: 10.1021/jp067009t

Trick, K., and Saliba, T. (1995). "Mechanisms of the pyrolysis of phenolic resin in a carbon/phenolic composite," *Carbon* 33(11), 1509-1515. DOI: 10.1016/0008-6223(95)00092-R

Zhang, D., Zhang, X., Chen, Y., Wang, C., and Ma, Y. (2012), "An environment-friendly route to synthesize reduced graphene oxide as a supercapacitor electrode material," *Electrochim. Acta* 69, 364-370. DOI: 10.1016/j.electacta.2012.03.024

Zhou, L., Zuo, Z., and Chow, M. (2005). "Danshen: An overview of its chemistry, pharmacology, pharmacokinetics, and clinical use," *J. Clin. Pharmacol.* 45(12), 1345-1359. DOI: 10.1177/0091270005282630

Zhu, H., Wang, X., Yang, F., and Yang, X. (2011), "Promising carbons for supercapacitors derived from fungi," *Adv. Mater.* 23(24), 2745-2748. DOI: 10.1002/adma.201100901